Title	First spectroscopic study of ^{51}Ar by the ($p,2p$) reaction
Author(s)	Juhász M. M., Elekes Z., Sohler D., Utsuno Yutaka, Yoshida Kazuki, Otsuka Takaharu, Ogata Kazuyuki, Doornenbal P., Obertelli A., Baba Hidetada, Browne F., Calvet D., Château F., Chen S., Chiga Nobuyuki, Corsi A., Cortés M. L., Delbart A., Gheller J.-M., Giganon A., Gillibert A., Hilaire C., Isobe T., Kobayashi Toshio, Kubota Yuki, Lapoux V., Motobayashi Toru, Murray I., Otsu Hideaki, Panin V., Paul N., Rodriguez W., Sakurai Hiroyoshi, Sasano Masaki, Steppenbeck D., Stuhl L., Sun Y. L., Togano Yasuhiro, Uesaka Tomohiro, Wimmer K., Yoneda Kenichiro, Achouri N. L., Aktas O., Aumann T., Chung L. X., Dombrádi Zs., Flavigny F., Franchoo S.,Gašparić I., Gerst R.-B., Gibelin J., Hahn K. I., Kim D., Koiwai Takuma, Kondo Yosuke, Koseoglou P., Lee J., Lehr C., Linh B. D., Liu H. N., Lokotko T., MacCormick M., Moschner K., Nakamura Takashi, Park S. Y., Rossi D., Sahin E., Söderström P.-A., Takeuchi Satoshi, Törnqvist H., Vaquero V., Wagner V., Wang S., Werner V., Xu X., Yamada Hiroki, Yan D., Yang Z., Yasuda Masahiro, Zanetti L.
Citation	Physics Letters B,814, p.136108_1-136108_8
Text Version	Published Journal Article
URL	https://jopss.jaea.go.jp/search/servlet/search?5070832
DOI	https://doi.org/10.1016/j.physletb.2021.136108
Right	©2021 The Author(s). Published by Elsevier B.V. This is an open access article under the CC BY license (http://creativecommons.org/licenses/by/4.0/). Funded by SCOAP³.

First spectroscopic study of ^{51}Ar by the (p,2p) reaction

M.M. Juhász [a,b], Z. Elekes [a,*], D. Sohler [a], Y. Utsuno [c,d], K. Yoshida [d], T. Otsuka [n,e,f],
K. Ogata [g,h], P. Doornenbal [n], A. Obertelli [n,i,j], H. Baba [n], F. Browne [n], D. Calvet [j], F. Château [j],
S. Chen [n,k,l], N. Chiga [n], A. Corsi [j], M.L. Cortés [n], A. Delbart [j], J.-M. Gheller [j], A. Giganon [j],
A. Gillibert [j], C. Hilaire [j], T. Isobe [n], T. Kobayashi [m], Y. Kubota [n,o], V. Lapoux [j],
T. Motobayashi [n], I. Murray [n,p], H. Otsu [n], V. Panin [n], N. Paul [j], W. Rodriguez [n,q,r],
H. Sakurai [n,s], M. Sasano [n], D. Steppenbeck [n], L. Stuhl [o], Y.L. Sun [i,j], Y. Togano [t], T. Uesaka [n],
K. Wimmer [s,n], K. Yoneda [n], N.L. Achouri [y], O. Aktas [u], T. Aumann [i,ab], L.X. Chung [v],
Zs. Dombrádi [a], F. Flavigny [p], S. Franchoo [p], I. Gašparić [n,w], R.-B. Gerst [x], J. Gibelin [y],
K.I. Hahn [z], D. Kim [n,z], T. Koiwai [s], Y. Kondo [aa], P. Koseoglou [i,ab], J. Lee [l], C. Lehr [i], B.D. Linh [v],
H.N. Liu [i,j,u], T. Lokotko [l], M. MacCormick [p], K. Moschner [x], T. Nakamura [aa], S.Y. Park [z],
D. Rossi [i,ab], E. Sahin [ac], P.-A. Söderström [n], S. Takeuchi [aa], H. Törnqvist [i,ab], V. Vaquero [ad],
V. Wagner [i], S. Wang [ae], V. Werner [i], X. Xu [l], H. Yamada [aa], D. Yan [ae], Z. Yang [n], M. Yasuda [aa],
L. Zanetti [i]

[a] *Atomki, Eötvös Loránd Research Network (ELKH), P.O. Box 51, H-4001 Debrecen, Hungary*
[b] *University of Debrecen, Egyetem tér 1, H-4032 Debrecen, Hungary*
[c] *Center for Nuclear Study, University of Tokyo, Hongo, Bunkyo-ku, Tokyo 113-0033, Japan*
[d] *Advanced Science Research Center, Japan Atomic Energy Agency, Tokai, Ibaraki 319-1195, Japan*
[e] *Department of Physics and Center for Nuclear Study, University of Tokyo, Hongo, Bunkyo-ku, Tokyo 113-0033, Japan*
[f] *Instituut voor Kern- en Stralingsfysica, Katholieke Universiteit Leuven, B-3001 Leuven, Belgium*
[g] *Research Center for Nuclear Physics (RCNP), Osaka University, Ibaraki 567-0047, Japan*
[h] *Department of Physics, Osaka City University, Osaka 558-8585, Japan*
[i] *Institut für Kernphysik, Technische Universität Darmstadt, 64289 Darmstadt, Germany*
[j] *IRFU, CEA, Université Paris-Saclay, F-91191 Gif-sur-Yvette, France*
[k] *State Key Laboratory of Nuclear Physics and Technology, Peking University, Beijing 100871, People's Republic of China*
[l] *Department of Physics, The University of Hong Kong, Pokfulam Road, Hong Kong*
[m] *Department of Physics, Tohoku University, Sendai 980-8578, Japan*
[n] *RIKEN Nishina Center, 2-1 Hirosawa, Wako, Saitama 351-0198, Japan*
[o] *Center for Nuclear Study, University of Tokyo, RIKEN campus, Wako, Saitama 351-0198, Japan*
[p] *Institut de Physique Nucléaire, IN2P3-CNRS, Université Paris-Sud, Université Paris-Saclay, 91406 Orsay Cedex, France*
[q] *Universidad Nacional de Colombia, Sede Bogota, Facultad de Ciencias, Departamento de Física, 111321, Bogotá, Colombia*
[r] *Pontificia Universidad Javeriana, Facultad de Ciencias, Departamento de Física, Bogotá, Colombia*
[s] *Department of Physics, University of Tokyo, 7-3-1 Hongo, Bunkyo, Tokyo 113-0033, Japan*
[t] *Department of Physics, Rikkyo University, 3-34-1 Nishi-Ikebukuro, Toshima, Tokyo 172-8501, Japan*
[u] *Department of Physics, Royal Institute of Technology, SE-10691 Stockholm, Sweden*
[v] *Institute for Nuclear Science & Technology, VINATOM, P.O. Box 5T-160, Nghia Do, Hanoi, Viet Nam*
[w] *Ruđer Bošković Institute, Bijenička cesta 54, 10000 Zagreb, Croatia*
[x] *Institut für Kernphysik, Universität zu Köln, D-50937 Cologne, Germany*
[y] *LPC Caen, ENSICAEN, Université de Caen, CNRS/IN2P3, F-14050 Caen, France*
[z] *Ewha Womans University, Seoul 120-750, Republic of Korea*
[aa] *Department of Physics, Tokyo Institute of Technology, 2-12-1 O-Okayama, Meguro, Tokyo, 152-8551, Japan*
[ab] *GSI Helmholtzzentrum für Schwerionenforschung GmbH, 64291 Darmstadt, Germany*
[ac] *Department of Physics, University of Oslo, N-0316 Oslo, Norway*
[ad] *Instituto de Estructura de la Materia, CSIC, E-28006 Madrid, Spain*
[ae] *Institute of Modern Physics, Chinese Academy of Sciences, Lanzhou 730000, People's Republic of China*

* Corresponding author.
  E-mail address: elekes@atomki.hu (Z. Elekes).

ABSTRACT

The nuclear structure of ^{51}Ar, an uncharted territory so far, was studied by the (p,2p) reaction using γ-ray spectroscopy for the bound states and the invariant mass method for the unbound states. Two peaks were detected in the γ-ray spectrum and six peaks were observed in the ^{50}Ar+n relative energy spectrum. Comparing the results to our shell-model calculations, two bound and six unbound states were established. Three of the unbound states could only be placed tentatively due to the low number of counts in the relative energy spectrum of events associated with the decay through the first excited state of ^{50}Ar. The low cross sections populating the two bound states of ^{51}Ar could be interpreted as a clear signature for the presence of significant subshell closures at neutron numbers 32 and 34 in argon isotopes. It was also revealed that due to the two valence holes, unbound collective states coexist with individual-particle states in ^{51}Ar.

1. Introduction

Working on the origin of the elements, Maria Goeppert-Mayer and Edward Teller discovered a specific pattern and special numbers in atomic nuclei later named *magic* by Eugene Wigner. In this context Goeppert-Mayer published her important work on the closed shells [1,2] which paved the way to a fertile field of nuclear physics. It was soon realized that these magic numbers were not static, the location of single-particle states might change, and as a consequence magicity could appear at numbers different from the conventional ones in certain regions of nuclei [3–5]. In the past decades concerted experimental and theoretical efforts have been made to uncover the change of magicity and its underlying mechanisms [6].

Based on the indirect (energy of the first 2^+ state, reduced transition strength, etc.) and direct (for example, two-neutron separation energy) indicators of magicity substantial experimental data were collected which supported a new magic number at $N = 32$ for Cr [7,8], Ti [9,10], Sc [11], Ca [12–14], K [15], and Ar [16] isotopes. However, contrary results were also published for Ti [17] isotopes showing the limitation of the indicators. In addition, a possible subshell closure at the neutron number 34 was also predicted as early as about 20 years ago [18]. This magicity did not manifest itself in Cr [8,7], Ti [9,19] and Sc [20] isotopes, however few experiments indicated its presence in Ca [21–23] and Ar [24] isotopes.

The low-lying structure of ^{53}Ca, located between $N = 32$ and $N = 34$ was investigated by β-decay [25], multi-nucleon knock-out [21] and neutron knock-out [23] reactions. The observed lowest two excited states ($3/2_1^-$, $5/2_1^-$) were interpreted by promoting a neutron to a higher orbital across the sizable shell gaps at 32 and 34, respectively. By removing two protons from ^{53}Ca we arrive at ^{51}Ar, which is a similar outstanding case to test the magicity of the neutron numbers 32 and 34. Therefore, we have studied ^{51}Ar for the first time by the (p,2p) reaction in order to map its low-lying excited states.

2. Experiment

The experiment was performed at the Radioactive Isotope Beam Factory operated by the RIKEN Nishina Center and the Center for Nuclear Study of the University of Tokyo. A beam of ^{70}Zn ions was produced at an energy of 345 MeV/u and at a beam intensity of 240 pnA by the accelerator complex. This primary stable beam collided with a ^{9}Be production target of 10 mm thickness placed at the entrance of the BigRIPS separator [26] forming radioactive nuclei by fragmentation. The selection of ions of interest was performed by the $B\rho - \Delta E - TOF$ method ($B\rho$: magnetic rigidity, ΔE: energy loss, *TOF*: time of flight) [27] using slits and

an aluminum wedged degrader at the first focal plane F1, located between the two dipole magnets D1 and D2 of BigRIPS. The constituents of the resulting cocktail beam were tagged between the focal planes F3 and F7 by time of flight, energy loss and magnetic rigidity measurements. The *TOF* was determined by plastic scintillators at F3 and F7 [28], while ΔE was taken from a gas ionization chamber at F7 [29]. The trajectory of the particles was monitored by several sets of parallel plate avalanche counters (PPAC) at F3, F5 and F7 [30,31].

The excited states of ^{51}Ar were produced in nucleon removal reactions using the MINOS device [32] which consisted of a polyethylene terephthalate cell filled with liquid hydrogen and a cylindrical time projection chamber (TPC) placed downstream of the focal plane F13. The effective target length was determined to be 151(1) mm. The TPC chamber contained a gas mixture of argon, CF_4 and isobutane at room temperature and atmospheric pressure. Its length, inner diameter, and outer diameter were 300 mm, 80 mm, and 178.8 mm, respectively. The point of reaction was reconstructed either by using the scattered and the removed protons or one of the protons and the projected trajectory of the radioactive ions (the former method was preferred when both data were available) [33]. An overall efficiency of 95% and a resolution of 5 mm (FWHM) along the beam axis was achieved for the events when at least one proton was recorded by the TPC.

The prompt γ rays were detected by the DALI2+ array [34] consisting of 226 NaI(Tl) scintillator crystals packed in cylindrical layers of 10-28 units around the liquid hydrogen target and a forward wall of 64 units. This arrangement provided a coverage of polar angles between 15° and 118°. The beam-like fragments leaving the target were analyzed by the SAMURAI spectrometer [35] based on $B\rho$, ΔE, and *TOF* measurements. The $B\rho$ values were derived via trajectory determination by multiwire drift chambers located upstream (FDC1) and downstream (FDC2) of the magnet operated at a central magnetic field of 2.7 T. Downstream of the FDC2 a plastic scintillator wall consisting of 24 bars yielded the ΔE and the *TOF* relative to a plastic detector at F13.

For the observation of excited states decaying by neutron emission, neutron *TOF* spectrometers NeuLAND and NEBULA were placed at 11 m and 14 m, respectively, downstream of the target at 0° [36]. NEBULA consisted of 120 plastic scintillator bars, each with a dimension of 12 cm(W)×12 cm(D)×180 cm(H) arranged in two walls. Both walls consisted of two layers and were equipped with an additional thin (1 cm) layer of plastic scintillators vetoing against the charged particles. The front face of the walls were separated by a distance of 85 cm. 400 NeuLAND units with a dimension of 5 cm(W)×5 cm(D)×250 cm(H) developed by the R³B collaboration [37] were placed upstream of NEBULA in 8 alternating horizontal and vertical layers to increase efficiency.

Approximately 200 particles hit the liquid hydrogen cell every second while the intensity of the ^{52}K ions was about 6 pps. The mean kinetic energy of the ^{52}K particles at the entrance of the target was measured to be 260 MeV/u, losing an average 83 MeV/u while passing through the liquid hydrogen. 894 and 4002 events were counted in the ^{52}K(p,2p)^{51}Ar and ^{52}K(p,2p)^{51}Ar$\rightarrow$^{50}Ar+n reaction channels, respectively.

3. Results and discussion

All the crystals of the DALI2+ array were calibrated for energy several times during the experiment using ^{60}Co, ^{137}Cs, and ^{88}Y radioactive sources, which allowed a correction for the gain shift of the detectors (<0.4%). In order to increase the photopeak efficiency of the setup, an addback procedure was applied during the analysis. This combined the hits in adjacent units (<15 cm) originating from a single γ ray undergoing Compton-scattering and/or pair production. The Doppler-correction of the emitted γ rays was performed using the vertex position determined by a tracking algorithm for protons in the TPC. The change of the drift velocity in the TPC was monitored during the experiment and was taken into account in the analysis.

Fig. 1 shows the Doppler-corrected experimental γ-ray spectra for ^{51}Ar fragments. In the upper panel, there was no selection on the incoming beam, so all the reaction channels were included while the lower panel shows the events for the ^{52}K(p,2p)^{51}Ar reaction channel. Three peaks seem to be present in the upper panel, the positions of which were determined at 809(16) keV, 963(9) keV, and 1180(9) keV by fitting the spectrum with Gaussian functions plus a double-exponential background. The uncertainties originated from the statistics and the uncertainty due to the energy calibration (5 keV). The peaks at 963 keV and 1180 keV also appear for the ^{52}K(p,2p)^{51}Ar reaction channel but the peak at 809 keV is barely visible.

In order to further analyze the spectra, separate simulations were performed for the three transitions with the GEANT4 code [38]. The resulting response functions were added together with individual scaling parameters plus a double-exponential background. The total fits are presented by red lines (including three peaks) in Fig. 1 while the backgrounds are plotted by blue lines. The statistical confidence of the peaks were determined to be 2.5σ, 8.7σ and 9.5σ for the three peaks in the upper panel, which indicates that the peak at 809 keV might not be real. For the lower panel, the confidence of this peak is even lower (1.0σ) and the χ^2_υ values showed that the spectra could be fitted with an assumption of only two peaks (green line in Fig. 1). Therefore, the peak at 809 keV was not considered further.

Due to the low statistics, $\gamma\gamma$ matrices could not be used to conclude coincidences for the γ rays, therefore we assumed that both transitions connected each an excited state and the ground state establishing two levels at energies of 963 keV and 1180 keV. The parallel placement of the γ rays is supported by the low neutron separation energy of ^{51}Ar ($S_n = 1.4(7)$ MeV from mass systematics [39], $S_n = 1.57$ MeV from our shell-model calculation). For the ^{52}K(p,2p)^{51}Ar reaction channel, the inclusive cross section was determined to be 0.62(2) mb while the exclusive cross section was extracted to be 0.046(14) mb and 0.102(18) mb for the 963-keV and the 1180-keV states, respectively.

The unbound excited states of ^{51}Ar populated by the (p,2p) reaction were derived by reconstructing the relative energy (E_{rel}) of the ^{50}Ar+neutron system. This energy is simply the difference between the invariant mass before and after the decay while the energy of the excited states can be calculated by adding the neutron separation energy of ^{51}Ar. For the relative energy, the momentum of the ^{50}Ar ions were determined by the SAMURAI spectrometer and the momentum of the neutron by the NEBULA+NeuLAND *TOF*
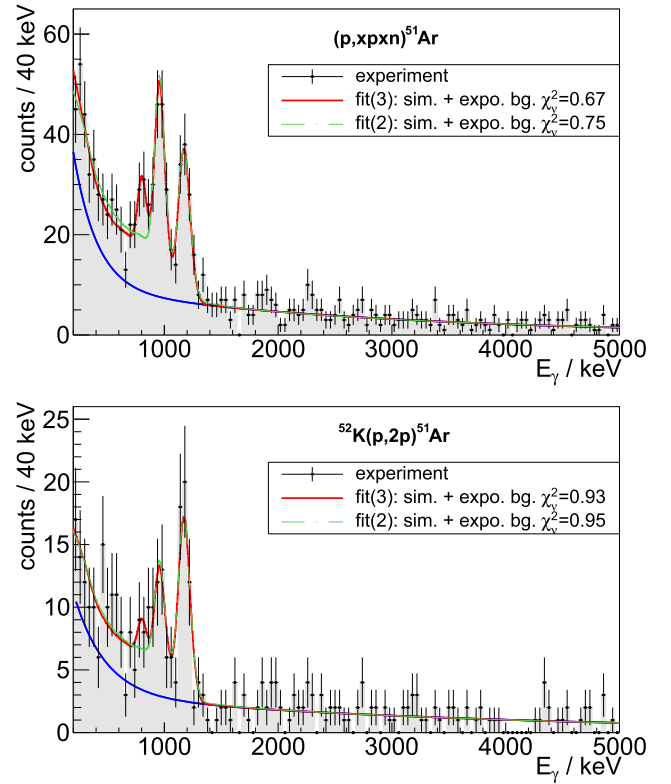

Fig. 1. Doppler-corrected γ-ray spectra for ^{51}Ar using vertex reconstruction (requiring only a single proton in the TPC) and addback procedure (upper panel: all reaction channels, lower panel: ^{52}K(p,2p)^{51}Ar reaction channel). The data with error bars and shaded area represent the experimental spectrum, the red and green lines are the simulations including three and two peaks, respectively, plus a double-exponential background, and the latter function (exponential background) is also plotted separately as a blue line.

spectrometer. The *TOF* calibration was performed using the γ-ray flash arriving at the spectrometer from the target before the neutrons. The unbound excited states of ^{51}Ar could decay in a way that either the ground state or the excited states of ^{50}Ar were produced. For the latter case, the emitted γ rays were also taken into account in order to correctly reconstruct the excited levels of ^{51}Ar.

The resulting relative energy spectra are shown in Fig. 2 where the counts were corrected for the neutron detection efficiency of the NEBULA+NeuLAND setup (55% at 100 keV, 20% at 5 MeV). The upper panel includes all the events from the decay of unbound states in ^{51}Ar while the lower panel was prepared with a gate on the $E_\gamma = 1.178$ MeV transition between the first excited state and the ground state of ^{50}Ar [16]. The resonances appearing in the spectra were fitted with Breit-Wigner functions [40] (lines of light green, light blue, magenta, cyan, dark green, dark blue) according to the R-matrix theory [41]. The particular form of the functions included a central resonance energy parameter (E_0), an energy-dependent apparent width parameter (Γ), an orbital angular momentum parameter of the resonance (l), and a scaling factor. On the other hand, a non-resonant contribution to the spectra could also arise which was modeled by a Maxwellian function (black line) [42] and added to the final fitting function (red line).

As a result, six resonances were identified the parameters of which are listed in Table 1. The best fit ($\chi^2_\upsilon = 0.99$) achieved with the l values in the Table, however, these could not be used for a definitive assignment since similar goodness of fit could be gained by different sets of orbital angular momentum parameters. In the lower panel only four peaks (271 keV, 1040 keV, 1494 keV, 1883 keV) out of the observed six seem to appear. This spectrum was fitted in a manner similar to the above men-
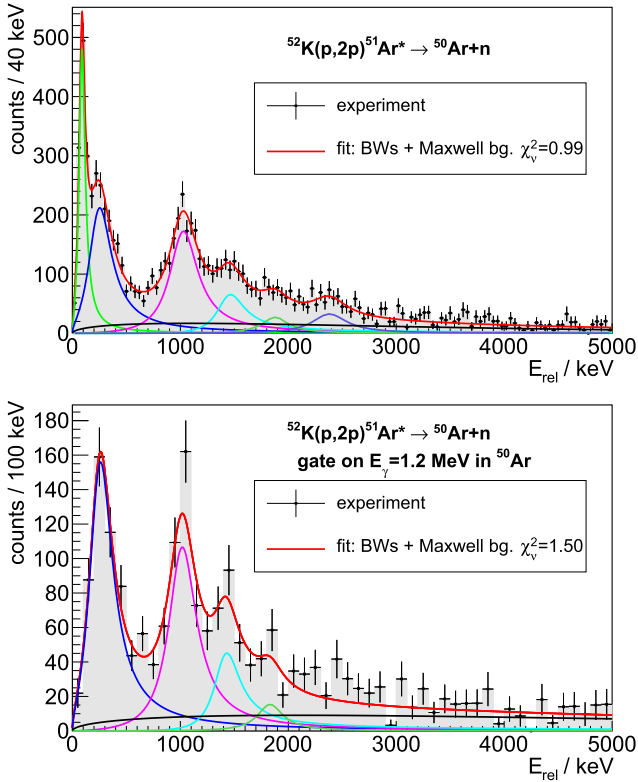
Fig. 2. Relative energy spectra for ^{51}Ar corrected for the energy-dependent neutron detection efficiency including all the events from the decay of the excited states (upper panel) and only those events which were in coincidence with the transition between the first excited state and the ground state of ^{50}Ar (lower panel). The data with error bars and shaded area represent the experimental spectrum. The red line represents a fit of Breit-Wigner functions (light green, light blue, magenta, cyan, dark green, dark blue) plus a background modeled by a Maxwell function. For the fit in the lower panel, the Breit-Wigner widths and positions were fixed to the values taken from the fit in the upper panel.

Table 1
Resonance parameters determined by fitting the spectrum of the ^{52}K(p,2p)^{51}Ar→^{50}Ar+n reaction channel. E_0 is the central resonance energy, Γ is the energy-dependent apparent width, l is the deduced orbital angular momentum of the resonance. The statistical confidence (C) of the peaks is also indicated.

E_0 (keV)	Γ (keV)	l	C
92(4)	69(11)	0	41.5σ
271(13)	272(37)	0	35.2σ
1040(12)	324(37)	1	47.8σ
1449(35)	361(156)	3	17.4σ
1883(56)	297(120)	1	7.9σ
2386(43)	391(172)	1	13.3σ

tioned one but keeping E_0, Γ and l fixed to the values derived from the fit of the spectrum in the upper panel. The $\chi_\nu^2 = 1.50$ value shows that our proposal of four resonances might be valid, however, the spectrum could also be fitted well with an assumption of three (271 keV, 1040 keV, 1494 keV) or even five (271 keV, 1040 keV, 1494 keV, 1883 keV, 2386 keV) peaks. In conclusion, this analysis unambiguously establishes an excited state at $E_1^x = S_n + 92$ keV decaying to the ground state of ^{50}Ar and two states at $E_2^x = S_n + 271$ keV $+ 1178$ keV $= S_n + 1449$ keV and $E_3^x = S_n + 1040$ keV $+ 1178$ keV $= S_n + 2218$ keV decaying through the first excited state in ^{50}Ar (1178 keV [16]). Due to the low statistics in the lower panel of Fig. 2, we can only tentatively establish the three other states at $E_4^x = S_n + 2386$ keV,

$E_5^x = S_n + 1494$ keV $+ 1178$ keV $= S_n + 2672$ keV and $E_6^x = S_n + 1883$ keV $+ 1178$ keV $= S_n + 3061$ keV. The exclusive cross sections for the six states were obtained to be 0.93(12) mb, 1.54(24) mb, 1.56(20) mb, 0.35(12) mb, 0.7(3) mb and 0.23(9) mb, respectively.

To compare the experimental findings with theory, shell-model calculations were performed in the sd-pf valence space employing effective interactions of SDPF-MUs Hamiltonian introduced in Ref. [43] which is based on the SDPF-MU Hamiltonian [44,45] fine-tuned to take into account experimental data in this region of nuclei, such as ^{49}K [46,47], ^{51}K, ^{53}K [43] and ^{54}Ca [21]. This new SDPF-MUs Hamiltonian includes a shift of the original $T = 0$ central force monopole strength between the proton $s_{1/2}$ and neutron $p_{1/2}$ orbitals as well as between the proton $s_{1/2}$ and neutron $p_{3/2}$ orbitals in order to better describe the experimental results for ^{51}K and ^{53}K. Additionally, the neutron $f_{5/2}^2$ pairing matrix element was also shifted a little to better match the 2^+ energies in the Ca isotopes. The spin/parity of the ground state of ^{52}K was not unambiguously determined experimentally. A β-decay study excluded the 0^-, and proposed the 2^- assignment [48] but the 1^- was also found to be possible by our shell-model calculations. Therefore, when dealing with the (p,2p) reaction, both the 1^- and the 2^- scenarios were considered.

The output of the shell-model calculations regarding the level and decay scheme is shown in the left part of Fig. 3. The characteristics of the theoretical states are listed in Table 2. Since the neutron separation energy is not known for ^{51}Ar, the calculated theoretical value of 1.57 MeV is plotted in Fig. 3, and the energy of the experimental states are also placed relative to this S_n. It is worth noting that the mass systematics gives a similar S_n of 1.4(7) MeV [39].

To compare the exclusive cross sections deduced from the experiment, we calculated the single-particle cross sections for the (p,2p) reaction within the distorted wave impulse approximation (DWIA) framework [49]. The single-particle wave function and the nuclear density were obtained by the Bohr-Mottelson single-particle potential [50]. The optical potentials for the distorted waves in the initial and final channels were constructed by the microscopic folding model [51] with the Melbourne g-matrix interaction [52] and the calculated nuclear density. The spin-orbit part of each distorting potential was disregarded, which introduced an uncertainty of about 5% for the cross sections. As for the pp interaction, the Franey-Love effective interaction [53] was adopted. These theoretical cross sections were combined with the spectroscopic factors of our shell-model calculations and averaged over the beam energy covered by our target similar to the experimental exclusive cross sections. The resulting theoretical cross sections with $J^\pi = 2^-$ (^{52}K g.s.) for the relevant states are listed in Table 3 and also indicated next to the levels in Fig. 3.

The shell-model calculations provide two bound excited states (975 keV, 1117 keV) which are very close in energy to the proposed observed levels (963 keV, 1180 keV). Moreover, the calculated cross sections are also in a fair agreement with the experimental ones. This suggests that our assumption, i.e., the observed transitions do not form a cascade but are parallel to each other, is valid. The small experimental cross sections (46 µb, 102 µb) show that these states are dominated by neutron excitations across the shell gaps at neutron numbers 32 and 34 since they are weakly populated by the (p,2p) reaction. Likewise, the observed inclusive cross section of 0.62(2) mb and the theoretical one of 1.15 mb agree reasonably well. However, we note that an assignment opposite to the one in Fig. 3 can not be excluded for the two bound states, i.e., $J^\pi = 5/2_1^-$ might belong to the observed 963-level and $J^\pi = 3/2_1^-$ to the observed 1180-level. This good match between the experimental results and the shell-model predictions suggests that the shell gaps at $N = 32$ and $N = 34$ are indeed large, as implied by the shell-model calculations, which is illustrated in Fig. 4
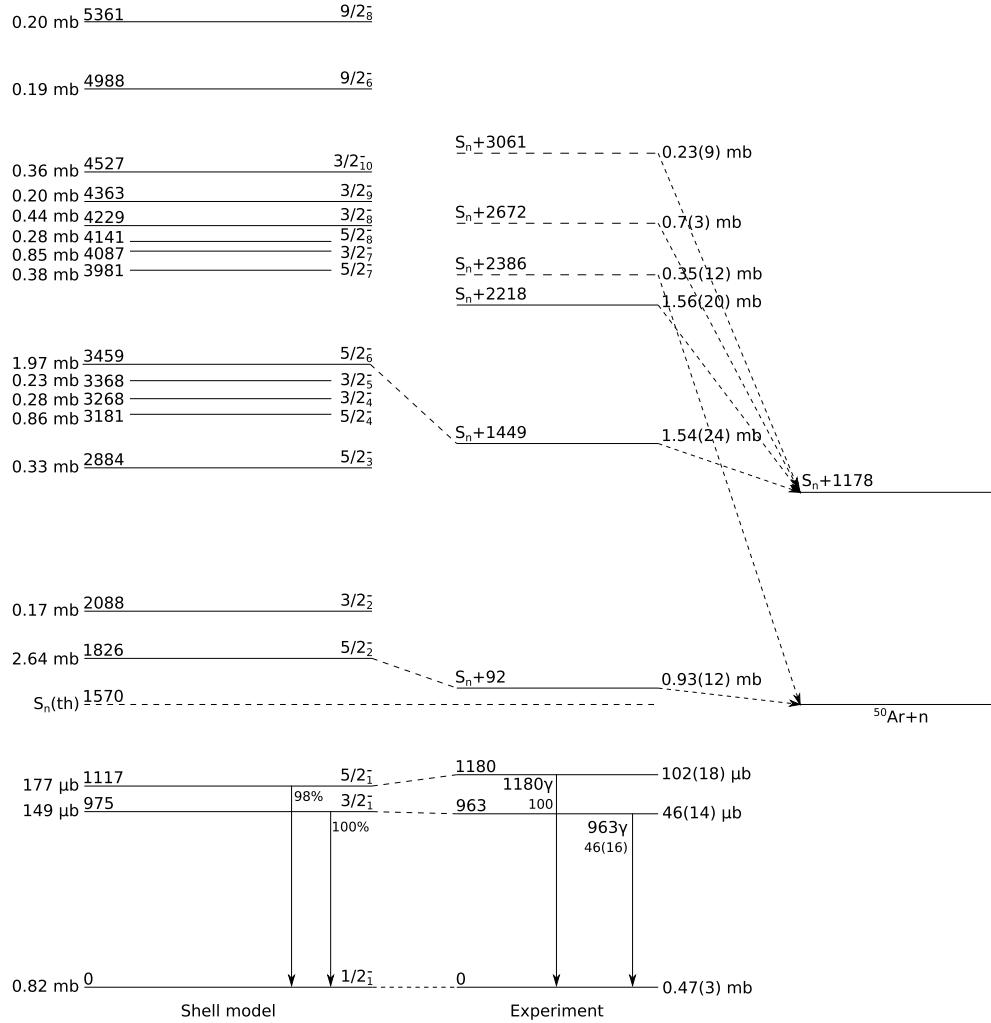
Fig. 3. Partial level and decay scheme of ^{51}Ar up to the expected two-neutron separation energy of 5.6(7) MeV [39]. The two observed bound excited states with their decay and relative γ-ray intensities corrected for the efficiency of the DALI2+ array are shown below the neutron separation energy of 1570 keV taken from our shell-model calculation. Three further unbound excited states were also established by the experiment and three tentatively placed excited states are also plotted with dashed lines together with their decay either to the ground state or the first excited states of ^{50}Ar. The numbers on the right hand side of the levels indicate the extracted exclusive cross section in the ^{52}K(p,2p)^{51}Ar reaction. The experimental data are compared with our shell-model calculations with $J^{\pi} = 2^-$ (^{52}K g.s.). The calculated γ-ray branching ratios are also written next to the downward arrows. Only those states are displayed for which the calculated (p,2p) cross section is above 0.1 mb. The four lowest excited states observed in the experiment could be matched with counterparts in the shell-model level scheme but it should be noted that the two bound states can also be assigned inversely to the theoretical ones. The cross section values left hand side of the theoretical levels were derived from the spectroscopic factors and the theoretical single-particle cross sections.

for the $N = 32$ isotones. As protons are removed from the proton $f_{7/2}$ orbital, the neutron $f_{5/2}$ orbital increases rapidly. The neutron $p_{3/2}$ and $p_{1/2}$ orbitals also moderately increase keeping their energy splitting nearly constant, and as a consequence sub-shell gaps at neutron numbers 32 and 34 emerge in Ca and Ar isotopes.

It is noted that the $J^{\pi} = 1^-$ (^{52}K g.s.) scenario gives similar results with a particular difference in the calculated cross section value of 709 μb for the $5/2_1^-$ level contradicting the experimental data, which supports the 2^- assignment for the ground state of ^{52}K.

Looking at the characteristics of the calculated unbound states in Table 2, it is obvious that the $5/2_2^-$ and $5/2_6^-$ levels significantly differ from the $5/2_1^-$ level (and from the other calculated $5/2^-$ levels) if we consider the z-component (taking $J_z = J$) of their angular momentum (L_z) values. For these two unbound states, the large L_z values indicate significant proton contribution to the excitation, which is also reflected in the sizable calculated cross sections (2.64 mb, 1.97 mb). We propose to assign our observed states at E_1^x

and E_2^x to the theoretical $5/2_2^-$ and $5/2_6^-$ levels, respectively based on the observed large cross sections (0.93(12) mb, 1.54(24) mb) comparable to the theoretical ones. Regarding the calculated unbound $3/2^-$ levels, it can be seen that all of them show somewhat more proton dominance over the $3/2_1^-$ one based on the L_z values. Besides, the $3/2_7^-$ state is notable because the z-component (taking $J_z = J$) of its spin (S_z) is also large. This also shows up in the calculated substantial cross section (0.85 mb). The energy and the cross section of the observed state (E_3^x, 1.56(20) mb) indicate that it might be the counterpart of the theoretical $3/2_7^-$ level however, due to the resolution in E_{rel}, it cannot be excluded that some other nearby theoretical levels contribute. The collective property of the mentioned higher-lying states (especially for $5/2_2^-$, $5/2_6^-$) can also be seen by comparing their calculated $B(E2)$ values of 53 e^{2}fm^4 and 14 e^{2}fm^4 to that of the individual-particle $5/2_1^-$ state of only 5 e^{2}fm^4. Such a collective behavior is also present for several higher-lying $3/2^-$ states but not so emphasized. For the remaining three other observed states, no corresponding theoretical levels can be determined because their energy is uncertain

Table 2

The z-component (taking $J_z = J$) of spin (S_z) and of angular momentum (L_z) together with the occupation number of nucleon orbitals for the theoretical states (E_{theor}) from our shell-model calculations. Only those excited states are shown for which the theoretical (p,2p) cross section exceeds 0.1 mb.

| E_{theor} (MeV)	J^π	Nucleon type	S_z	L_z	Orbits						
					$d_{5/2}$	$d_{3/2}$	$s_{1/2}$	$f_{7/2}$	$f_{5/2}$	$p_{3/2}$	$p_{1/2}$
0	$1/2_1^-$	π	−0.004	0.025	5.83	2.46	1.72	0	0	0	0
		ν	−0.131	0.610	6	4	2	7.78	0.40	3.77	1.04
0.975	$3/2_1^-$	π	−0.014	0.216	5.82	2.65	1.53	0	0	0	0
		ν	0.243	1.055	6	4	2	7.69	0.47	3.18	1.67
1.117	$5/2_1^-$	π	−0.009	0.199	5.78	2.66	1.56	0	0	0	0
		ν	−0.181	2.491	6	4	2	7.58	1.22	3.25	0.95
1.826	$5/2_2^-$	π	−0.046	1.439	5.83	2.68	1.49	0	0	0	0
		ν	−0.185	1.291	6	4	2	7.69	0.68	3.59	1.04
2.088	$3/2_2^-$	π	−0.016	0.785	5.77	2.80	1.43	0	0	0	0
		ν	0.131	0.599	6	4	2	7.42	1.53	3.23	0.82
2.884	$5/2_3^-$	π	−0.007	0.344	5.79	2.73	1.48	0	0	0	0
		ν	0.062	2.101	6	4	2	7.53	1.43	3.03	1.01
3.181	$5/2_4^-$	π	−0.036	0.373	5.79	2.66	1.55	0	0	0	0
		ν	−0.073	2.236	6	4	2	7.43	1.25	3.34	0.99
3.268	$3/2_4^-$	π	−0.091	0.924	5.83	2.60	1.57	0	0	0	0
		ν	0.095	0.572	6	4	2	7.59	0.91	3.44	1.05
3.368	$3/2_5^-$	π	−0.033	0.848	5.85	2.61	1.54	0	0	0	0
		ν	0.059	0.626	6	4	2	7.70	0.88	3.09	1.33
3.459	$5/2_6^-$	π	−0.081	1.269	5.86	2.67	1.47	0	0	0	0
		ν	−0.132	1.443	6	4	2	7.67	0.83	3.53	0.97
3.980	$9/2_2^-$	π	−0.037	1.261	5.78	2.59	1.63	0	0	0	0
		ν	−0.066	3.342	6	4	2	7.46	1.28	3.42	0.85
3.981	$5/2_7^-$	π	−0.016	0.914	5.82	2.75	1.43	0	0	0	0
		ν	−0.002	1.605	6	4	2	7.53	1.14	3.10	1.22
4.087	$3/2_7^-$	π	−0.219	0.908	5.85	2.89	1.26	0	0	0	0
		ν	0.025	0.787	6	4	2	7.54	1.26	3.33	0.87
4.137	$9/2_3^-$	π	−0.019	1.043	5.76	2.74	1.51	0	0	0	0
		ν	0.153	3.323	6	4	2	7.20	1.75	3.11	0.94
4.141	$5/2_8^-$	π	−0.010	0.616	5.81	2.75	1.44	0	0	0	0
		ν	−0.171	2.065	6	4	2	7.46	1.38	3.03	1.14
4.229	$3/2_8^-$	π	−0.174	0.798	5.87	2.75	1.38	0	0	0	0
		ν	0.067	0.810	6	4	2	7.63	0.92	3.37	1.09
4.363	$3/2_9^-$	π	−0.048	0.368	5.81	2.80	1.39	0	0	0	0
		ν	0.033	1.147	6	4	2	7.51	1.23	3.01	1.25
4.527	$3/2_{10}^-$	π	−0.060	0.367	5.89	2.88	1.23	0	0	0	0
		ν	0.102	1.090	6	4	2	7.75	0.66	3.23	1.36
4.988	$9/2_6^-$	π	−0.067	1.068	5.78	2.57	1.65	0	0	0	0
		ν	−0.135	3.635	6	4	2	7.60	1.35	3.23	0.82
5.361	$9/2_8^-$	π	−0.004	0.707	5.73	2.70	1.57	0	0	0	0
		ν	−0.068	3.865	6	4	2	7.30	1.73	3.09	0.87
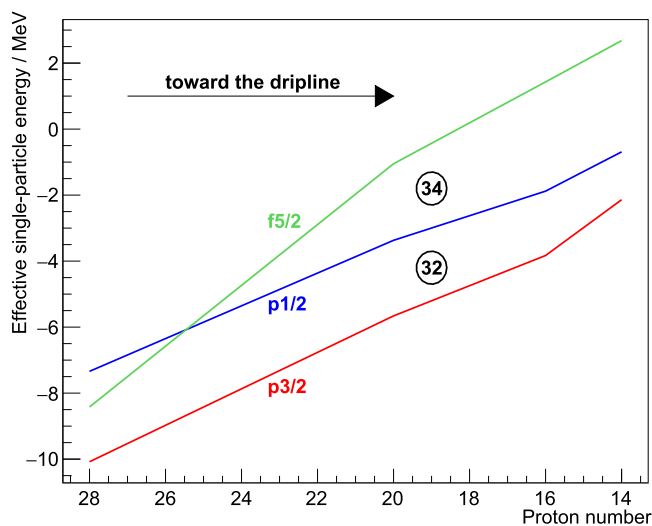
Fig. 4. Change of effective single-particle orbitals at $N = 32$ as the proton number decreases toward the dripline.

due to their questionable existence in the E_{rel} spectrum in coincidence with the 1178-keV γ ray in ^{50}Ar as well as the density of theoretical states at high energies.

4. Summary

The ^{51}Ar, lying between the possible $N = 32$ and $N = 34$ subshell closures predicted by theoretical calculations and suggested by some earlier experimental works, was studied via the (p,2p) reaction. Its low-lying level structure, unexplored until now, was established using γ-ray spectroscopy and the invariant mass method. The observed two bound states were populated very weakly which is a clear indication that they are mainly formed by promoting a neutron across the shell gaps at $N = 32$ and $N = 34$. Therefore, this is in line with the previous results [16,24], i.e., the subshells gaps at $N = 32$ and $N = 34$ are substantial in argon isotopes. Some of the detected unbound states were populated with large cross sections, which turned out to have collective behavior according to our shell model calculations. This means that ^{51}Ar is an atomic nucleus in which individual-particle and collective states coexist.

Declaration of competing interest

The authors declare that they have no known competing financial interests or personal relationships that could have appeared to influence the work reported in this paper.

Table 3

Theoretical level energies (E_{theor}), spectroscopic factors, exclusive cross sections for the reaction ^{52}K(p,2p)^{51}Ar (σ_{theor}) in comparison with experimental level energies (E_{expt}) and cross sections (σ_{expt}) up to the expected two neutron separation energy of 5.6(7) MeV [39]. The level energies and spectroscopic factors originate from our shell-model calculations with $J^\pi = 2^-$ (^{52}K g.s.) while the cross sections are obtained by combining the DWIA cross sections and the spectroscopic factors. The uncertainty in the DWIA framework and its input is about 20% as discussed in Ref. [49]. Only those excited states are shown for which the theoretical (p,2p) cross section exceeds 0.1 mb. Regarding the experimental data, four states could be matched with theoretical levels. However, the assignments of the lowest two excited states are ambiguous since they can be swapped.

E_{theor} (MeV)	J^π	Spectroscopic factor		σ_{theor} (mb)	E_{expt} (MeV)	σ_{expt} (mb)
0	$1/2_1^-$	<0.01	$d_{5/2}$	0.82	0	0.47(3)
		0.37	$d_{3/2}$			
0.975	$3/2_1^-$	<0.01	$d_{5/2}$	0.149	0.963(9)	0.046(14)
		0.04	$d_{3/2}$			
		0.02	$s_{1/2}$			
1.117	$5/2_1^-$	0.07	$d_{5/2}$	0.177	1.180(9)	0.102(18)
		<0.01	$d_{3/2}$			
		<0.01	$s_{1/2}$			
1.826	$5/2_2^-$	0.01	$d_{5/2}$	2.64	$S_n + 0.092(4)$	0.93(12)
		0.67	$d_{3/2}$			
		0.38	$s_{1/2}$			
2.088	$3/2_2^-$	0.06	$d_{5/2}$	0.17		
		0.01	$d_{3/2}$			
		0.01	$s_{1/2}$			
2.884	$5/2_3^-$	<0.01	$d_{5/2}$	0.33		
		0.14	$d_{3/2}$			
		0.01	$s_{1/2}$			
3.181	$5/2_4^-$	<0.01	$d_{5/2}$	0.86		
		0.37	$d_{3/2}$			
		0.03	$s_{1/2}$			
3.268	$3/2_4^-$	<0.01	$d_{5/2}$	0.28		
		0.13	$d_{3/2}$			
		<0.01	$s_{1/2}$			
3.368	$3/2_5^-$	<0.01	$d_{5/2}$	0.23		
		0.09	$d_{3/2}$			
		0.01	$s_{1/2}$			
3.459	$5/2_6^-$	<0.01	$d_{5/2}$	1.97	$S_n + 1.449(35)$	1.54(24)
		0.49	$d_{3/2}$			
		0.31	$s_{1/2}$			
3.980	$9/2_2^-$	<0.09	$d_{5/2}$	0.20		
3.981	$5/2_7^-$	<0.01	$d_{5/2}$	0.38		
		0.03	$d_{3/2}$			
		0.11	$s_{1/2}$			
4.087	$3/2_7^-$	<0.01	$d_{5/2}$	0.85		
		0.02	$d_{3/2}$			
		0.28	$s_{1/2}$			
4.137	$9/2_3^-$	0.05	$d_{5/2}$	0.11		
4.141	$5/2_8^-$	<0.01	$d_{5/2}$	0.28		
		0.08	$d_{3/2}$			
		0.03	$s_{1/2}$			
4.229	$3/2_8^-$	<0.01	$d_{5/2}$	0.44		
		<0.01	$d_{3/2}$			
		0.15	$s_{1/2}$			
4.363	$3/2_9^-$	<0.01	$d_{5/2}$	0.20		
		<0.01	$d_{3/2}$			
		0.06	$s_{1/2}$			
4.527	$3/2_{10}^-$	<0.01	$d_{5/2}$	0.36		
		<0.01	$d_{3/2}$			
		0.11	$s_{1/2}$			
4.988	$9/2_6^-$	0.08	$d_{5/2}$	0.19		
5.361	$9/2_8^-$	0.09	$d_{5/2}$	0.20		

References

[1] M.G. Mayer, Phys. Rev. 74 (1948) 235.

[2] M.G. Mayer, Phys. Rev. 75 (1949) 1969.

[3] I. Talmi, I. Unna, Phys. Rev. Lett. 4 (1960) 469.

[4] C. Thibault, R. Klapisch, C. Rigaud, A.M. Poskanzer, R. Prieels, L. Lessard, W. Reisdorf, Phys. Rev. C 12 (1975) 644.

[5] B. Bastin, S. Grévy, D. Sohler, O. Sorlin, Z. Dombrádi, N.L. Achouri, J.C. Angélique, F. Azaiez, D. Baiborodin, R. Borcea, et al., Phys. Rev. Lett. 99 (2007) 022503.

[6] T. Otsuka, A. Gade, O. Sorlin, T. Suzuki, Y. Utsuno, Rev. Mod. Phys. 92 (2020) 015002.

[7] A. Bürger, T. Saito, H. Grawe, H. Hübel, P. Reiter, J. Gerl, M. Górska, H. Wollersheim, A. Al-Khatib, A. Banu, et al., Phys. Lett. B 622 (2005) 29.

[8] J. Prisciandaro, P. Mantica, B. Brown, D. Anthony, M. Cooper, A. Garcia, D. Groh, A. Komives, W. Kumarasiri, P. Lofy, et al., Phys. Lett. B 510 (2001) 17.

[9] D.-C. Dinca, R.V.F. Janssens, A. Gade, D. Bazin, R. Broda, B.A. Brown, C.M. Campbell, M.P. Carpenter, P. Chowdhury, J.M. Cook, et al., Phys. Rev. C 71 (2005) 041302.

[10] R. Janssens, B. Fornal, P. Mantica, B. Brown, R. Broda, P. Bhattacharyya, M. Carpenter, M. Cinausero, P. Daly, A. Davies, et al., Phys. Lett. B 546 (2002) 55.

[11] X. Xu, M. Wang, Y.-H. Zhang, H.-S. Xu, P. Shuai, X.-L. Tu, Y.A. Litvinov, X.-H. Zhou, B.-H. Sun, Y.-J. Yuan, et al., Chin. Phys. C 39 (2015) 104001.

[12] F. Wienholtz, D. Beck, K. Blaum, C. Borgmann, M. Breitenfeldt, R.B. Cakirli, S. George, F. Herfurth, J.D. Holt, M. Kowalska, et al., Nature 498 (2013) 346.

[13] A. Huck, G. Klotz, A. Knipper, C. Miehé, C. Richard-Serre, G. Walter, A. Poves, H.L. Ravn, G. Marguier, Phys. Rev. C 31 (1985) 2226.

[14] A. Gade, R.V.F. Janssens, D. Bazin, R. Broda, B.A. Brown, C.M. Campbell, M.P. Carpenter, J.M. Cook, A.N. Deacon, D.-C. Dinca, et al., Phys. Rev. C 74 (2006) 021302.

[15] M. Rosenbusch, P. Ascher, D. Atanasov, C. Barbieri, D. Beck, K. Blaum, C. Borgmann, M. Breitenfeldt, R.B. Cakirli, A. Cipollone, et al., Phys. Rev. Lett. 114 (2015) 202501.

[16] D. Steppenbeck, S. Takeuchi, N. Aoi, P. Doornenbal, M. Matsushita, H. Wang, Y. Utsuno, H. Baba, S. Go, J. Lee, et al., Phys. Rev. Lett. 114 (2015) 252501.

[17] E. Leistenschneider, M.P. Reiter, S. Ayet San Andrés, B. Kootte, J.D. Holt, P. Navrátil, C. Babcock, C. Barbieri, B.R. Barquest, J. Bergmann, et al., Phys. Rev. Lett. 120 (2018) 062503.

[18] T. Otsuka, R. Fujimoto, Y. Utsuno, B.A. Brown, M. Honma, T. Mizusaki, Phys. Rev. Lett. 87 (2001) 082502.

[19] S.N. Liddick, P.F. Mantica, R.V.F. Janssens, R. Broda, B.A. Brown, M.P. Carpenter, B. Fornal, M. Honma, T. Mizusaki, A.C. Morton, et al., Phys. Rev. Lett. 92 (2004) 072502.

[20] D. Steppenbeck, S. Takeuchi, N. Aoi, P. Doornenbal, M. Matsushita, H. Wang, H. Baba, S. Go, J.D. Holt, J. Lee, et al., Phys. Rev. C 96 (2017) 064310.

[21] D. Steppenbeck, S. Takeuchi, N. Aoi, P. Doornenbal, M. Matsushita, H. Wang, H. Baba, N. Fukuda, S. Go, M. Honma, et al., Nature 502 (2013) 207.

[22] S. Michimasa, M. Kobayashi, Y. Kiyokawa, S. Ota, D.S. Ahn, H. Baba, G.P.A. Berg, M. Dozono, N. Fukuda, T. Furuno, et al., Phys. Rev. Lett. 121 (2018) 022506.

[23] S. Chen, J. Lee, P. Doornenbal, A. Obertelli, C. Barbieri, Y. Chazono, P. Navrátil, K. Ogata, T. Otsuka, F. Raimondi, et al., Phys. Rev. Lett. 123 (2019) 142501.

[24] H.N. Liu, A. Obertelli, P. Doornenbal, C.A. Bertulani, G. Hagen, J.D. Holt, G.R. Jansen, T.D. Morris, A. Schwenk, R. Stroberg, et al., Phys. Rev. Lett. 122 (2019) 072502.

[25] F. Perrot, F. Maréchal, C. Jollet, P. Dessagne, J.-C. Angélique, G. Ban, P. Baumann, F. Benrachi, U. Bergmann, C. Borcea, et al., Phys. Rev. C 74 (2006) 014313.

[26] T. Kubo, D. Kameda, H. Suzuki, N. Fukuda, H. Takeda, Y. Yanagisawa, M. Ohtake, K. Kusaka, K. Yoshida, N. Inabe, et al., Prog. Theor. Exp. Phys. 2012 (2012), 03C003.

[27] T. Kubo, in: 14th International Conference on Electromagnetic Isotope Separators and Techniques Related to Their Applications, Nucl. Instrum. Methods Phys. Res., Sect. B, Beam Interact. Mater. Atoms 204 (2003) 97.

[28] N. Fukuda, T. Kubo, T. Ohnishi, N. Inabe, H. Takeda, D. Kameda, H. Suzuki, Nucl. Instrum. Methods Phys. Res., Sect. B, Beam Interact. Mater. Atoms 317 (2013) 323.

[29] K. Kimura, T. Izumikawa, R. Koyama, T. Ohnishi, T. Ohtsubo, A. Ozawa, W. Shinozaki, T. Suzuki, M. Takahashi, I. Tanihata, et al., Nucl. Instrum. Methods Phys. Res., Sect. A, Accel. Spectrom. Detect. Assoc. Equip. 538 (2005) 608.

[30] H. Kumagai, A. Ozawa, N. Fukuda, K. Sümmerer, I. Tanihata, Nucl. Instrum. Methods Phys. Res., Sect. A, Accel. Spectrom. Detect. Assoc. Equip. 470 (2001) 562.

[31] H. Kumagai, T. Ohnishi, N. Fukuda, H. Takeda, D. Kameda, N. Inabe, K. Yoshida, T. Kubo, Nucl. Instrum. Methods Phys. Res., Sect. B, Beam Interact. Mater. Atoms 317 (2013) 717.

[32] A. Obertelli, A. Delbart, S. Anvar, L. Audirac, G. Authelet, H. Baba, B. Bruyneel, D. Calvet, F. Château, A. Corsi, et al., Eur. Phys. J. A 50 (2014) 8.

[33] C. Santamaria, A. Obertelli, S. Ota, M. Sasano, E. Takada, L. Audirac, H. Baba, D. Calvet, F. Château, A. Corsi, et al., Nucl. Instrum. Methods Phys. Res., Sect. A, Accel. Spectrom. Detect. Assoc. Equip. 905 (2018) 138.

[34] S. Takeuchi, T. Motobayashi, Y. Togano, M. Matsushita, N. Aoi, K. Demichi, H. Hasegawa, H. Murakami, Nucl. Instrum. Methods Phys. Res., Sect. A, Accel. Spectrom. Detect. Assoc. Equip. 763 (2014) 596.

[35] T. Kobayashi, N. Chiga, T. Isobe, Y. Kondo, T. Kubo, K. Kusaka, T. Motobayashi, T. Nakamura, J. Ohnishi, H. Okuno, et al., in: XVIth International Conference on ElectroMagnetic Isotope Separators and Techniques Related to Their Applications, December 2-7, 2012, Matsue, Japan, Nucl. Instrum. Methods Phys. Res., Sect. B, Beam Interact. Mater. Atoms 317 (2013) 294.

[36] Y. Kondo, T. Tomai, T. Nakamura, Nucl. Instrum. Methods Phys. Res., Sect. B, Beam Interact. Mater. Atoms 463 (2020) 173.

[37] T. Aumann, et al., R³B technical design report for NeuLAND, https://edms.cern.ch/ui/file/1865739/1/TDR_R3B_NeuLAND_public.pdf, 2011. (Accessed 22 September 2020).

[38] S. Agostinelli, J. Allison, K. Amako, J. Apostolakis, H. Araujo, P. Arce, M. Asai, D. Axen, S. Banerjee, G. Barrand, et al., Nucl. Instrum. Methods Phys. Res., Sect. A, Accel. Spectrom. Detect. Assoc. Equip. 506 (2003) 250.

[39] M. Wang, G. Audi, F.G. Kondev, W. Huang, S. Naimi, X. Xu, Chin. Phys. C 41 (2017) 030003.

[40] G. Breit, E. Wigner, Phys. Rev. 49 (1936) 519.

[41] A.M. Lane, R.G. Thomas, Rev. Mod. Phys. 30 (1958) 257.

[42] K. Le Couteur, D. Lang, Nucl. Phys. 13 (1959) 32.

[43] Y. Sun, A. Obertelli, P. Doornenbal, C. Barbieri, Y. Chazono, T. Duguet, H. Liu, P. Navrátil, F. Nowacki, K. Ogata, et al., Phys. Lett. B (ISSN 0370-2693) 802 (2020) 135215.

[44] Y. Utsuno, T. Otsuka, B.A. Brown, M. Honma, T. Mizusaki, N. Shimizu, Phys. Rev. C 86 (2012) 051301.

[45] Y. Utsuno, T. Otsuka, Y. Tsunoda, N. Shimizu, M. Honma, T. Togashi, T. Mizusaki, JPS Conf. Proc. 6 (2015) 010007.

[46] R. Broda, J. Wrzesiński, A. Gadea, N. Mărginean, B. Fornal, L. Corradi, A.M. Stefanini, W. Królas, T. Pawłat, B. Szpak, et al., Phys. Rev. C 82 (2010) 034319.

[47] J. Papuga, M.L. Bissell, K. Kreim, K. Blaum, B.A. Brown, M. De Rydt, R.F. Garcia Ruiz, H. Heylen, M. Kowalska, R. Neugart, et al., Phys. Rev. Lett. 110 (2013) 172503.

[48] F. Perrot, F. Maréchal, C. Jollet, P. Dessagne, J.-C. Angélique, G. Ban, P. Baumann, F. Benrachi, U. Bergmann, C. Borcea, et al., Phys. Rev. C 74 (2006) 014313.

[49] T. Wakasa, K. Ogata, T. Noro, Prog. Part. Nucl. Phys. 96 (2017) 32.

[50] A. Bohr, B. Mottelson, Nuclear Structure, vol. I, Benjamin, New York, 1969.

[51] M. Toyokawa, K. Minomo, M. Yahiro, Phys. Rev. C 88 (2013) 054602.

[52] K. Amos, P. Dortmans, H. von Geramb, S. Karataglidis, J. Raynal, Adv. Nucl. Phys. 25 (2000) 275.

[53] M.A. Franey, W.G. Love, Phys. Rev. C 31 (1985) 488.